Kinetics of the polymer collapse transition: The role of hydrodynamics

N. Kikuchi,* J. F. Ryder, C. M. Pooley,† and J. M. Yeomans
Rudolf Peierls Centre for Theoretical Physics, 1 Keble Road, Oxford, OX1 3NP, United Kingdom
(Received 20 September 2004; published 30 June 2005)

We investigate numerically the dynamical behavior of a polymer chain collapsing in a dilute solution. The rate of collapse is measured with and without the presence of hydrodynamic interactions. We find that hydrodynamic interactions accelerate polymer collapse. We present a scaling theory describing the physical process responsible for the collapse kinetics. Predicted collapse times in a hydrodynamic ($\tau_H \sim N^{4/3}$) and a Brownian heat bath ($\tau_B \sim N^2$) agree well with the numerical results ($\tau_H \sim N^{1.40\pm0.08}$ and $\tau_B \sim N^{1.89\pm0.09}$) where N denotes chain length. The folding kinetics of Go models of proteins is also examined. We show that for these systems, where many free energy minima compete, hydrodynamics has little effect on the kinetics.

DOI: 10.1103/PhysRevE.71.061804 PACS number(s): 83.80.Rs, 82.20.Wt, 82.35.Lr

I. INTRODUCTION

When the temperature is lowered rapidly or the solvent quality is changed from good to poor, the resulting effective attractive interactions between monomers can cause a polymer to undergo a collapse transition (coil-globule transition) from a swollen to a compact state. The equilibrium properties of the polymer transition from the swollen to the collapsed state are well understood [1,2]. However, the kinetics of the transition and in particular the effect on that kinetics of the hydrodynamic properties of the solvent are less clear.

In a previous paper we presented an investigation of the kinetics of the polymer collapse transition [3]. The collapse was monitored with and without the presence of hydrodynamic interactions, therefore allowing a direct investigation of including backflow. We found that hydrodynamics speeds up the polymer collapse. Here we extend that work, giving numerical results for longer chains and evidence for our interpretation that the collapsing polymer sets up a flow which, in turn, speeds up its collapse. We also present a scaling theory describing the physical picture responsible for the collapse kinetics. We explore the effect of excluded volume on the collapse. We then consider simple models of protein folding and show that for these hydrodynamics has little effect on the folding kinetics.

Understanding the kinetics of the polymer collapse transition is a challenging task. Experimentally it is difficult because accessible concentration and length-time scales are limited [4–8]. For the available concentrations there is significant competition between intrachain collapse and interchain aggregation.

Theoretical work on the dynamics of polymer collapse can be broadly divided into two approaches. Following de Gennes [9] several authors have developed phenomenological models which balance the driving and dissipative forces to give scaling laws [10–17]. However, these require assumptions about how the collapsed state develops on which there is no consensus. Other approaches have been based on solutions of the Langevin equation [18–22]. Of particular interest is work by Pitard [18] and by Kuznetsov *et al.* [19] who find the inclusion of hydrodynamics, modeled by a preaveraged Oseen tensor, speeds up the collapse. However, the values predicted in the literature for the exponents ν relating the collapse time to the chain length ($\tau_H \sim N^\nu$) vary widely.

Early simulations on polymer collapse [10,15,23,24], using Monte Carlo or Langevin approaches, also led to diverging interpretations. Moreover, they did not include the hydrodynamic effects of the solvent. However, recent work has shown that it is now possible to use molecular dynamics simulations with an explicit solvent to model the collapse transition if powerful computational resources are available [17,25]. Chang and Yethiraj [25] compared molecular dynamics simulations of a polymer in a solvent to Brownian dynamics simulations for short chains of up to 128 monomers. Abrahams *et al.* [17] simulated chains of length 512 using a molecular dynamics approach for both polymer and solvent. Further discussion of these papers is given in Sec. VII.

Here we use a hybrid numerical approach to investigate polymer collapse and, in particular, the role of backflow on the collapse kinetics [26]. The solvent is modeled by a mesoscale algorithm, stochastic rotation dynamics [27], and the polymer by molecular dynamics as summarized in Sec. II. In Sec. III we present results for the dependence of the collapse time on the number of monomers for a chain in a Brownian and in a hydrodynamic solvent. In Sec. IV the exponents are reproduced using a simple scaling theory motivated by the simulations. We then explore, in Sec. V, the effect of including excluded volume between the monomers and solvent particles. We show that this change in the algorithm has no effect on the collapse kinetics. In Sec. VI we turn our attention to the role of hydrodynamics in the folding kinetics of proteins in dilute solution. We simulate a protein using a Go model [28–32] and show that for this system, where many free energy minima compete, hydrodynamics has little effect on the kinetics. Finally a conclusion summarizes the paper and discusses related literature.

*Now at Institut für Physik, Johannes Gutenberg-Universität Mainz, Staudinger Weg 7, D-55099 Mainz, Germany.
†Now at Chemical and Petroleum Engineering Department, 1249 Benedum Hall, Pittsburgh, PA 15261, USA.

II. MODEL

Modeling a dilute polymer solution is a difficult task because of the existence of widely differing time scales. The dynamical properties of polymers can be dominated by hydrodynamic interactions between different parts of the polymer chain [1,2,33,34]. In contrast to the time scale of thermal fluctuations of individual monomers, these interactions are long ranged and evolve slowly. Therefore it is computationally very expensive to reach hydrodynamic time scales using molecular dynamics simulations for both the polymer and solvent.

To overcome these problems we use a hybrid simulation approach [26] where the equations of motion of the polymer are solved using a molecular dynamics algorithm. The solvent is modeled using the stochastic rotation dynamics model [27]. This is a particle-based, mesoscopic model for simulating fluctuating hydrodynamics. It ignores the molecular detail of the solvent but preserves its ability to transmit hydrodynamic forces. The polymer can be thought of as moving within a "hydrodynamic heat bath."

The polymer chain is modeled by beads connected via springs [25,35] with the distance between adjacent beads along the chain backbone representing an effective Kuhn length (persistence length). The finitely extensible springs are represented by the FENE (finitely extensible nonlinear elastic) potential

$$V_{\mathrm{FENE}}(r) = -\frac{\kappa}{2}R_0^2 \ln\left[1-\left(\frac{r}{R_0}\right)^2\right], \quad r < R_0, \tag{1}$$

where r is the distance between the two monomers and R_0 denotes the maximum extension of the spring.

To mimic a good solvent a shifted Lennard-Jones potential which acts between all the polymer beads is used to model the excluded volume of the monomers [25,36]:

$$V_{\mathrm{LJ}}^{\mathrm{good}}(r) = \begin{cases} 4\varepsilon\left[\left(\frac{\sigma}{r}\right)^{12}-\left(\frac{\sigma}{r}\right)^{6}\right]+\varepsilon, & r \leqslant 2^{1/6}\sigma, \\ 0, & r > 2^{1/6}\sigma. \end{cases} \tag{2}$$

Note that this potential is purely repulsive.

To mimic a poor solvent a Lennard-Jones potential [25,36] which acts between all the polymer beads is employed to model both the volume exclusion of the monomers and a long-range attraction which drives the polymer collapse:

$$V_{\mathrm{LJ}}^{\mathrm{poor}}(r) = 4\varepsilon\left[\left(\frac{\sigma}{r}\right)^{12}-\left(\frac{\sigma}{r}\right)^{6}\right]. \tag{3}$$

Following Kremer and Grest [35], we take $\varepsilon=1.0$, $\sigma=1.0$, $\kappa=30\varepsilon/\sigma^2$, and $R_0=1.5\,\sigma$ where parameters are quoted in reduced Lennard-Jones units. The parameter $R_0=1.5\,\sigma$ in the FENE potential avoids possible bond crossing [35].

Newton's equations of motion for the polymer are integrated using the time-reversible velocity Verlet algorithm [36]. The molecular dynamics (MD) time step is chosen to be $\delta t_{\mathrm{MD}}=0.002\,\delta t$ where δt is the interval between solvent collision steps, defined in Eq. (4).

The solvent is modeled by a large number $N=131\,072$ of pointlike particles of mass m which move in continuous space with a continuous distribution of velocities, but discretely in time [27,37]. The algorithm proceeds in two steps. In the first of these, a free-streaming step, the positions of the solvent particles at time t, $\boldsymbol{r}_i(t)$, are updated simultaneously according to

$$\boldsymbol{r}_i(t+\delta t) = \boldsymbol{r}_i(t) + \boldsymbol{v}_i(t)\,\delta t, \tag{4}$$

where $\boldsymbol{v}_i(t)$ is the velocity of the particle and δt is the value of the discretized time step of the solvent which we take to be unity.

The second part of the algorithm is the collision step which is executed on both solvent particles and polymer beads. The system is coarse grained into a cubic grid with L^3/a^3 cells, which have side $a=1$. In these simulations $L=32$ is used. There is no restriction on the total number of solvent particles in each cell (although the total number of particles in the system is conserved). Stochastic multiparticle collisions are performed within each individual cell by rotating the velocity of each particle relative to the center-of-mass velocity $\boldsymbol{v}_{c.m.}(t)$ of all the particles within that cell:

$$\boldsymbol{v}_i(t+\delta t) = \boldsymbol{v}_{c.m.}(t) + \boldsymbol{R}(\boldsymbol{v}_i(t) - \boldsymbol{v}_{c.m.}(t)). \tag{5}$$

$\boldsymbol{R}$ is a rotation matrix which rotates velocities by a fixed angle α ($0<\alpha\leqslant\pi$) around an axis generated randomly for each cell and at each time step.

The volume in phase space is invariant under both the free-streaming and collision operations. Therefore the system is described by a microcanonical distribution at equilibrium [27]. The initial solvent distribution was generated by assigning positions randomly within the system with an average number of particles per unit cell, γ. The velocities were taken from a uniform distribution ($-v_{\max}\leqslant v_\alpha \leqslant v_{\max}$), $\alpha=x$, y, z, where $v_{\max}=\sqrt{3k_BT/m}$. The distribution relaxed rapidly (in ~ 100 time steps) to the equilibrium Maxwell-Boltzmann form corresponding to the temperature T. Note that the net momentum in the system must be set to zero [37].

Ihle and Kroll [38] pointed out that at low temperatures the transport coefficients of the stochastic rotation dynamics solvent show anomalies. This is because of the breakdown of the assumption of molecular chaos as particles undergo consecutive collisions within the same cell. Ihle and Kroll showed that it is possible to greatly improve the behavior of the algorithm by placing the cubic grid in a random position at each collision step. This correction has been included in the algorithm used here.

We note that the collision step preserves the position of the solvent and polymer beads. It transfers momentum between the polymer and solvent particles within a given cell while total momentum and energy are conserved. The thermohydrodynamic equations of motion are captured in the continuum limit [27]. Hence hydrodynamic interactions can be propagated by the solvent and, because the polymer beads are involved in the collisions, to the polymer. Note that it has been shown that the expected dynamic scaling laws (Zimm scaling) for, for example, the polymer center-of-mass diffusion coefficient hold for the model [26,39,40].

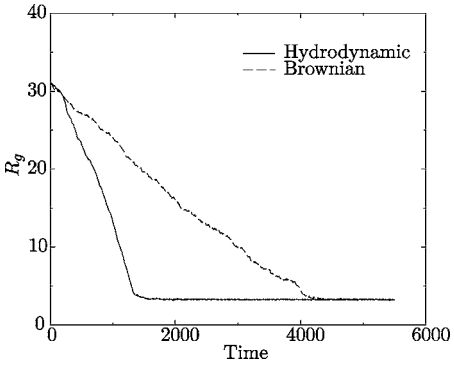

FIG. 1. Variation of the radius of gyration with time for a collapsing polymer in a hydrodynamic or Brownian heat bath for a chain of length $N=300$ at a final temperature $k_BT=0.8$. Axes are labeled in simulation units.

A particularly useful feature of stochastic rotation dynamics is the ease with which hydrodynamic interactions can be "turned off," thus replacing the hydrodynamic heat bath by a Brownian (random) heat bath. This is achieved by randomly interchanging the velocities of all the solvent particles after each collision step, thus relaxing the constraint of momentum conservation from a local to a global one. Accordingly the velocity correlations which result in hydrodynamic interactions disappear from the fluid although the equilibrium Maxwell-Boltzmann distribution is maintained. Running simulations with the same initial conditions and parameter values, but with hydrodynamics present or absent, greatly facilitates pinpointing the effects of the hydrodynamics [3].

III. HOMOPOLYMER COLLAPSE IN THE PRESENCE OF HYDRODYNAMIC INTERACTIONS

Our aim in this section is to study numerically the kinetics of polymer collapse from a swollen to a compact state [2]. Focusing on the role of hydrodynamics we show how the backflow speeds up the collapse kinetics. In the present calculations we take the mean solvent particle number $\gamma=4.0$, the mass of the solvent, $m=4.0$, and monomer, $M=16.0$, and the rotation angle $\alpha=90°$ [3]. The collapse transition is driven by the attractive Lennard-Jones interactions between the polymer beads [Eq. (3)]. The transition is rounded and shifted by the finite chain length, and takes place at $k_BT \sim 3.5$ for chains of length $N=100$.

Following Chang and Yhethiraj [25], polymer chains are equilibrated in good solvent conditions [Eq. (2)], for 10 000 solvent time steps (i.e., 5 000 000 MD time steps), then suddenly quenched into a poor solvent at $k_BT=0.8$. For convenience we set this time to zero. This value ensures collapse but prevents the chain collapsing so quickly that hydrodynamic interactions do not have sufficient time to develop. The rate of polymer collapse was measured by monitoring the variation of the radius of gyration R_g of the chain with time:

$$R_g^2 = \frac{1}{N}\sum_{i=1}^{N} (\mathbf{R}_i - \mathbf{R}_{c.m.})^2, \tag{6}$$

where $\mathbf{R}_i$ is the position of the ith monomer, N is the number of monomers, and $\mathbf{R}_{c.m.}$ is the position of the center of mass of the polymer chain:

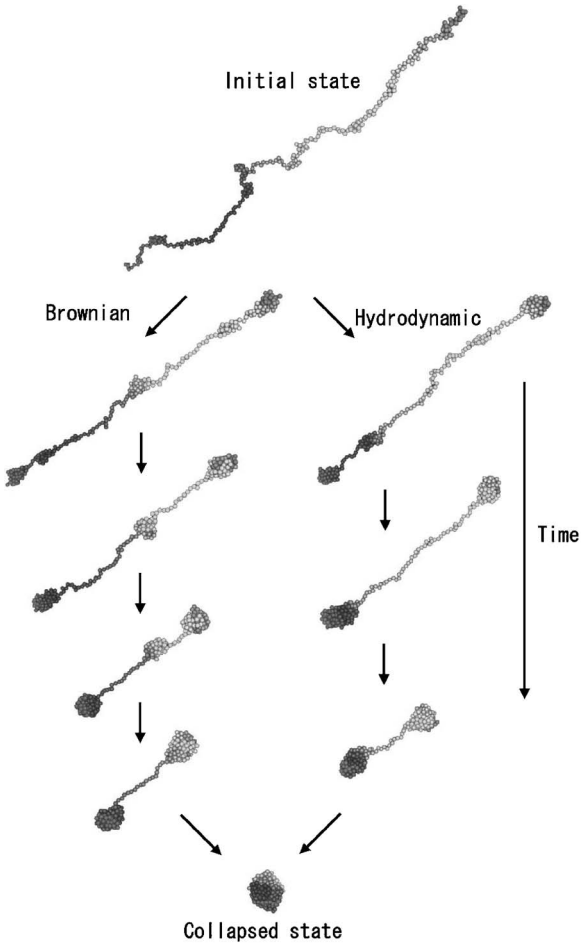

FIG. 2. A comparison of the pathways for polymer collapse with and without hydrodynamics for a polymer chain of length $N=300$ at a final temperature $k_BT=0.8$.

$$\mathbf{R}_{c.m.} = \frac{1}{N}\sum_{i=1}^{N} \mathbf{R}_i. \tag{7}$$

A typical numerical result for the variation of the radius of gyration with time with and without hydrodynamics is shown in Fig. 1 for a chain of length $N=300$. Note that the final radius of gyration was recorded for both the Brownian and hydrodynamic collapses and found to be the same as expected, as the equilibrium polymer properties should be independent of the nature of the heat bath.

The collapse time τ was identified when the radius of gyration first satisfied

$$R_g(t) = \frac{1}{100}(R_g(0) - \langle R_g \rangle_{\mathrm{eq}}) + \langle R_g \rangle_{\mathrm{eq}}, \tag{8}$$

where $\langle R_g \rangle_{\mathrm{eq}}$ is the equilibrium radius of gyration in the collapsed state. Results for τ are shown for chains of varying lengths in Table I. τ was averaged over 40 statistically independent initial configurations for $N=40$, 60, and 100, 30 for $N=200$, and 15 for $N=300$, and the collapse time for hydrodynamic (τ_H) and Brownian (τ_B) heat baths compared. Variations in collapse times between different runs are large as

TABLE I. Averaged collapse time in units of the solvent time step δt of a polymer chain of length N with (τ_H) and without (τ_B) hydrodynamics at $k_BT=0.8$. The radius of gyration after collapse in reduced Lennard-Jones units with ($\langle R_g\rangle_{\mathrm{eq}\ H}$) and without ($\langle R_g\rangle_{\mathrm{eq}\ B}$) hydrodynamics is also listed.

N	τ_H	τ_B	$\langle R_g\rangle_{\mathrm{eq}\ H}$	$\langle R_g\rangle_{\mathrm{eq}\ B}$
40	116±29	136±33	1.708±0.008	1.708±0.008
60	184±31	252±56	1.937±0.006	1.937±0.006
100	332±56	586±84	2.278±0.004	2.279±0.006
200	829±72	1999±211	2.844±0.003	2.844±0.003
300	1538±107	4421±318	3.246±0.005	3.258±0.010

expected. However, it is striking that hydrodynamic interactions speed up the rate of collapse for each polymer length. For $N=40$, 26 of the 40 runs and for $N=60$, 34 of the 40 runs collapsed faster with hydrodynamics switched on. For longer N all the hydrodynamic runs were faster.

The results in Table I also show that the collapse time increases with chain length as expected. The exponents are $\tau_H \sim N^{1.40\pm0.08}$ and $\tau_B \sim N^{1.89\pm0.09}$.

Figure 2 compares typical collapse pathways with and without hydrodynamics for a chain with $N=300$, at $k_BT=0.8$. In these and the majority of other runs little visible difference was observed in the collapse mechanism. After the quench the polymer very rapidly forms pearls (blobs) connected by linear segments as observed by other authors [17]. The pearls then absorb the monomer chains joining them, resulting in the contraction of the polymer to a collapsed state.

We expect the increased speed of collapse in a hydrodynamic solvent to result from solvent-pearl velocity correlations. When a pearl absorbs a monomer energy is liberated and the pearl receives a net force. This force will be the same for hydrodynamic and Brownian heat baths. However, in a hydrodynamic solvent the movement of pearls is enhanced by the flow of the surrounding fluid.

To investigate the solvent-pearl velocity correlation we considered a collapsed pearl of $N_p=60$ in equilibrium. The pearl was dragged by a force f_x applied to the monomer $i=N_p/2$. We measured the equal-time pearl-solvent velocity-velocity correlation $\langle \boldsymbol{V}_p(t)\cdot\boldsymbol{u}_s(t)\rangle$ and the average velocities of the pearl $\langle \boldsymbol{V}_p(t)\rangle$ and of the surrounding solvent $\langle \boldsymbol{u}_s(t)\rangle$ in a hydrodynamic and Brownian solvent.

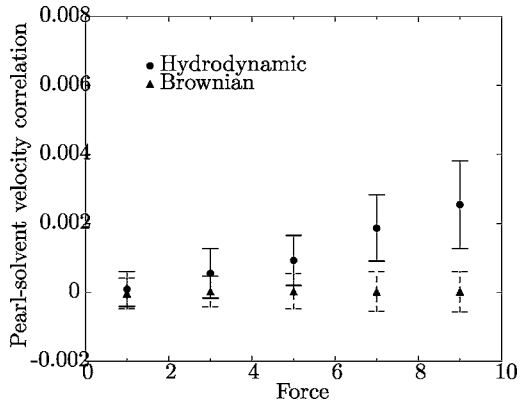

FIG. 3. Pearl-solvent velocity-velocity correlation as a pearl is dragged through a hydrodynamic and a Brownian heat bath for a polymer chain of length $N=60$ at temperature $k_BT=0.8$. Axes are labeled in simulation units.

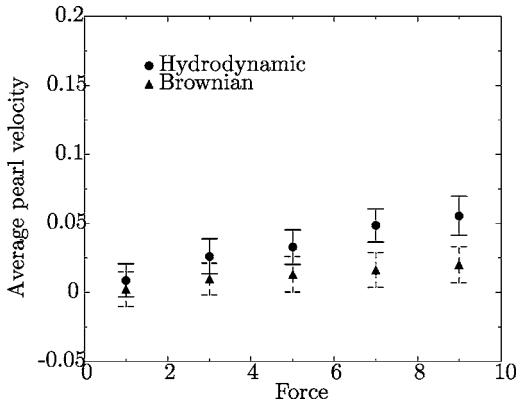

FIG. 4. Average velocity of a pearl dragged through a hydrodynamic and a Brownian heat bath for a polymer chain of length $N=60$ at temperature $k_BT=0.8$. Axes are labeled in simulation units.

Figure 3 shows the equal-time pearl-solvent velocity-velocity correlation in both heat baths. In a Brownian heat bath the pearl-solvent velocity correlation is zero as expected. We note, however, that there are velocity correlations in a hydrodynamic solvent. These correlations make it easier for the pearl to move and hence speed up the kinetics of polymer collapse in a hydrodynamic heat bath.

The average velocities of the pearl of radius R and that of the surrounding solvent within a sphere of radius R^3 are shown in Figs. 4 and 5, respectively. We observed a nonzero average velocity of the solvent in a hydrodynamic heat bath. In contrast the Brownian solvent velocity is zero. Since the movement of the pearl is supported by the hydrodynamic flow, its average velocity is larger in a hydrodynamic solvent (Fig. 4).

IV. SCALING ARGUMENT FOR THE COLLAPSE TIME

We now present a simple scaling argument predicting how the collapse time of a homopolymer depends on its length

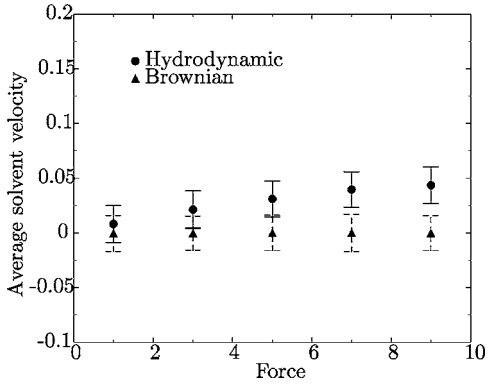

FIG. 5. Average velocity of the solvent around a moving pearl dragged through a hydrodynamic and a Brownian heat bath for a polymer chain of length $N=60$ at temperature $k_BT=0.8$. Axes are labeled in simulation units.

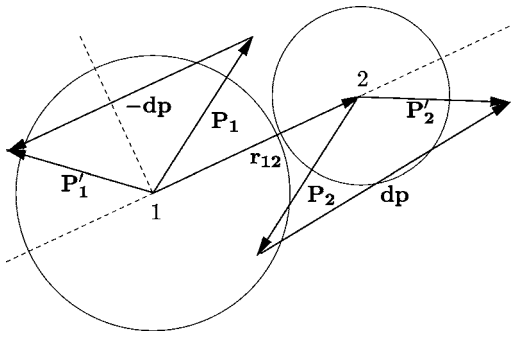

FIG. 6. A schematic diagram representing an elastic collision. Two particles 1 and 2 are colliding elastically in the center-of-mass frame.

[40]. We compare the behavior of polymers in a Brownian and a hydrodynamic heat bath.

After the quench the polymer very rapidly forms pearls connected by linear segments. The pearls then absorb the remaining monomers, resulting in the contraction of the polymer to form a collapsed state. The formation of pearls is relatively fast; for the longest chains studied it took approximately 5% of the total collapse time and in an explicit solvent-polymer molecular dynamics simulation [17] less than 3% for $N=512$. Therefore the collapse kinetics is dominated by the movement of the pearls (Fig. 2).

Consider two pearls connected by a string of monomers. When a pearl absorbs a monomer energy $\sim\varepsilon$ is liberated. Hence pearls receive a net force f from the string. On dimensional grounds,

$$f \sim \frac{\varepsilon}{\sigma}, \tag{9}$$

where σ is the diameter of a monomer.

In a Brownian solvent the pearl moves with terminal velocity

$$V_p^B = \frac{f}{N_p \xi}, \tag{10}$$

where ξ is a friction coefficient and N_p is the number of monomers that make up the pearl.

In a hydrodynamic solvent the average velocity of a dragged pearl V_p^H in a viscous fluid is

$$V_p^H = \frac{f}{C_1 \eta R}, \tag{11}$$

where η is the solvent shear viscosity and $R \sim \sigma N_p^{1/3}$ is the radius of the pearl. The numerical factor C_1 depends on the shape of the dragged object: for a sphere $C_1 = 6\pi$. For our simulations the data in Fig. 6 give $C_1 = (7.61 \pm 0.06)\pi$. η follows from the formula given in [37].

Since pearls absorb the monomers on the string, N_p changes in time according to

$$\frac{dN_p}{dt} = \frac{V_p}{\sigma}. \tag{12}$$

Solving Eq. (12) using the hydrodynamic (11) and Brownian (10) velocities and substituting expression (9) for f gives the growth law for the number of a beads in each pearl:

$$N_p^H \sim \left(\frac{\varepsilon}{\eta\sigma^3}\right)^{3/4} t^{3/4}, \tag{13}$$

$$N_p^B \sim \left(\frac{\varepsilon}{\sigma^2 \xi}\right)^{1/2} t^{1/2}. \tag{14}$$

When the number of monomers in each pearl is of order the total number of monomers in the chain we obtain the collapse time τ:

$$\tau_H \sim \left(\frac{\eta\sigma^3}{\varepsilon}\right) N^{4/3}, \tag{15}$$

$$\tau_B \sim \left(\frac{\sigma^2 \xi}{\varepsilon}\right) N^2, \tag{16}$$

which should be compared to the numerical results in Sec. III, $\tau_H \sim N^{1.40\pm0.08}$ and $\tau_B \sim N^{1.89\pm0.09}$.

We also note that the result for τ_H obtained here agrees with that given by Lee and Obukov [41] for a neutral polyelectrolyte.

V. EFFECT OF EXCLUDED VOLUME

In the algorithm described in Sec. II the monomers are transparent to the solvent particles. Here we describe an extension to the algorithm which enforces an excluded volume between the solvent particles and the monomers which make up the polymer chain.

We find that the change in algorithm has no effect on the collapse kinetics. This is as we expected, as the chain behavior depends on having a momentum transfer between polymer and solvent, not on the details of how this transfer takes place.

In real systems excluded-volume interactions will be important in the final stages of collapse as solvent molecules are trapped within the collapsed polymer. However, this is a regime where details of the molecular interactions are also very important and where our model is not valid.

Consider two colliding particles 1 and 2 (Fig. 6). In the center-of-mass frame the momentum of particles 1 and 2 are updated by elastic scattering to

$$\mathbf{P}_1' = \mathbf{P}_1 - \mathbf{dp},$$

$$\mathbf{P}_2' = \mathbf{P}_2 + \mathbf{dp}, \tag{17}$$

where $\mathbf{P}_i$ and $\mathbf{P}_i'$ denote the momentum before and after the elastic collisions, respectively ($i=1,2$). From Fig. 6,

$$\mathbf{dp} = 2\left(\frac{\mathbf{P}_1 \cdot \mathbf{r}_{12}}{r_{12}}\right)\frac{\mathbf{r}_{12}}{r_{12}} = \left(\frac{2m_1m_2}{m_1+m_2}\right)\frac{1}{{r_{12}}^2}[(\mathbf{v}_1 - \mathbf{v}_2)\cdot\mathbf{r}_{12}]\mathbf{r}_{12}, \tag{18}$$

where m_i is the particle mass, $\mathbf{v}_i$ is the velocity of the particle i, and r_{12} denotes the distance between the two particles. Elastic scattering is executed if the solvent particle overlaps a monomer after the streaming step:

$$r_{12} < (r_1 + r_2), \tag{19}$$

where r_i is the radius of particle i, and if the particles are moving towards each other,

$$(\boldsymbol{v}_1 - \boldsymbol{v}_2)\cdot\boldsymbol{r}_{12} > 0. \tag{20}$$

We take $r_1 = \sigma/2$ for the monomer and $r_2 = 0$ representing a pointlike solvent particle.

Simulations are performed as follows: first the monomer positions and velocities are updated using molecular dynamics. The solvent then streams. If solvent particles and monomers overlap, the elastic scattering collision is executed. The collision step (5) is then performed on the remaining solvent particles. The addition of an excluded-volume constraint increases the computational time by a factor of ~ 2.

The kinetics of polymer collapse was monitored with and without hydrodynamics using this algorithum to impose an excluded volume. The parameters used were the same as those given in Sec. III except for a mean particle number $\gamma = 10.0$.

Since we use a different coupling rule, the value of the friction acting on the monomer is changed for a given parameter set. Therefore it was not possible to make a quantitative comparison. However, there was no change in the qualitative form of the folding pathways and, as before, the collapse was speeded up by backflow effects.

VI. PROTEIN FOLDING

Given the effect of hydrodynamics on polymer collapse it is of interest to ask whether similar effects are seen in simple models of protein folding. The main new feature in proteins is the existence of a convoluted free energy surface. Model proteins are easily trapped in local minima, making it difficult for them to achieve the lowest-energy state (native state) [42].

We consider the Go Hamiltonian. This is one of the simplest coarse-grained models of proteins and it has been widely used to investigate their equilibrium and dynamical properties [28–32]. The Go Hamiltonian is constructed from the native state of a protein assuming that native interactions play an important role in the folding kinetics. It neglects unknown intramolecular interactions between amino acids.

The target native-state conformation is described by beads, representing amino acids, connected by springs. The springs are modeled by

$$V_s(r_{i,i+1}) = \kappa_1(r_{i,i+1} - d_0)^2 + \kappa_2(r_{i,i+1} - d_0)^4, \tag{21}$$

where $d_0 = 3.8$ Å, $\kappa_1 = \varepsilon$, and $\kappa_2 = 100\ \varepsilon$. ε denotes the depth of the Lennard-Jones potential given below.

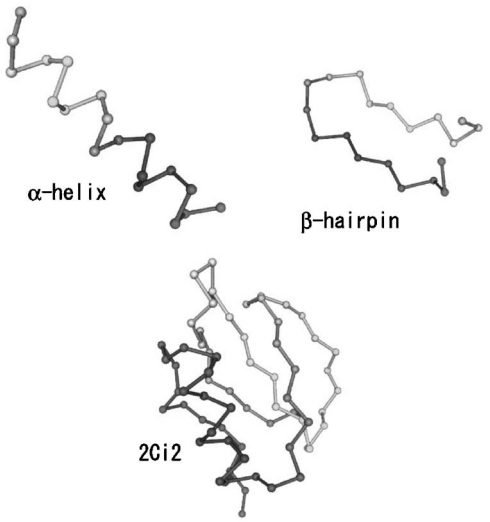

FIG. 7. Native states for an α-helix, a β-hairpin, and a protein $2ci2$.

To model native contact interactions between specific beads a Lennard-Jones potential is employed:

$$V_{\mathrm{nat}}(r_{i,j}) = 4\varepsilon\left[\left(\frac{\sigma_{i,j}}{r_{i,j}}\right)^{12} - \left(\frac{\sigma_{i,j}}{r_{i,j}}\right)^{6}\right], \tag{22}$$

where $\sigma_{i,j} = 2^{-1/6}d_{i,j}$. $d_{i,j}$ denotes the distances between the carbon-α of native contact pairs in the native state which are taken from the Protein Data Bank [43]. For non-native contact pairs a shifted Lennard-Jones potential is used:

$$V_{\mathrm{non}}(r_{i,j}) = \begin{cases} 4\varepsilon\left[\left(\dfrac{\sigma_0}{r_{i,j}}\right)^{12} - \left(\dfrac{\sigma_0}{r_{i,j}}\right)^{6}\right] + \varepsilon, & r_{i,j} \leqslant d_{\mathrm{cut}}, \\ 0, & r_{i,j} > d_{\mathrm{cut}}, \end{cases} \tag{23}$$

where $\sigma_0 = 2^{-1/6}d_{\mathrm{cut}}$. $d_{\mathrm{cut}} = \langle d_{i,j}\rangle$ is the mean value of all contact pair distances in the native state.

Newton's equations of motion for the protein were integrated using molecular dynamics. The protein was coupled to the stochastic rotation dynamics solvent as described in Sec. II. The mean solvent particle number was $\gamma = 5.0$, the mass of the solvent, $m = 1.0$, and monomer, $M = 16.0$, the rotation angle $\alpha = \pi/2$, and the system size was $L = 32$.

Statistically independent swollen chain configurations were placed in a solvent at equilibrium with $k_BT/\varepsilon = 0.1$, and the folding kinetics was monitored for 100 000 time steps. We examined a folding α-helix ($N = 19$), a β-hairpin ($N = 19$), and a protein $2ci2$ ($N = 65$). Native states are shown in Fig. 7. Here 20 runs were performed for each chain. Figures 8 and 9 show the collapse trajectories of the folding β-hairpin and the protein $2ci2$ in a hydrodynamic heat bath. For the β-hairpins folding took place through a zipping mechanism.

The rate of folding kinetics was measured by monitoring the variation of the radius of gyration, R_g, with time. There was no obvious difference between hydrodynamic and Brownian heat baths for any of the proteins considered. The

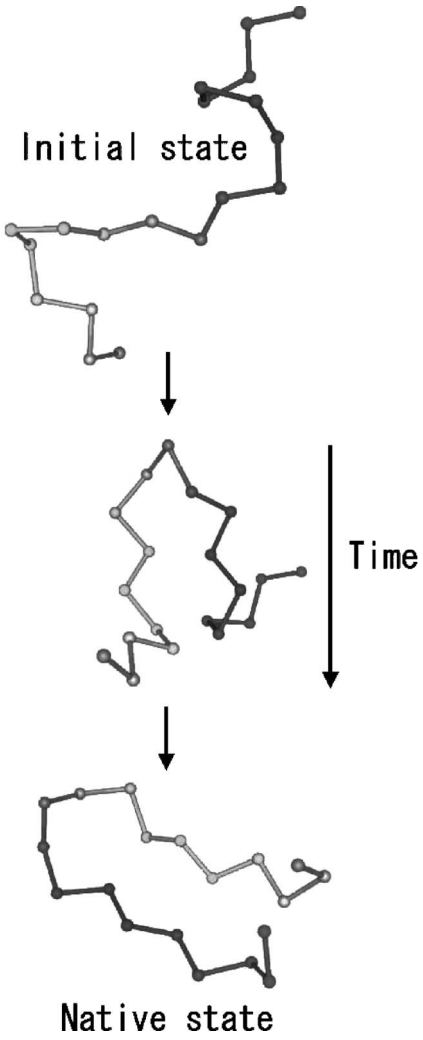

FIG. 8. A folding pathway for a β-hairpin.

model proteins escape from local trapping minima of the free energy through thermal noise. This process is not helped by hydrodynamics. Hydrodynamics tends to support the kinetics only when beads locally move in the same direction. This is not generally the case for a protein escaping from a free energy minimum, as the free energy landscape is so complex.

VII. DISCUSSION

Qualitative features of the collapse pathways for short chains ($N \sim 100$) are in agreement with those reported by Chang and Yethiraj [25] (see their Figs. 6 and 11) who recently compared molecular dynamics simulations of a polymer in a solvent, which included hydrodynamics, to Brownian dynamics simulations, which did not. These authors found that the Brownian simulations could become trapped in a metastable free energy minimum. We do not see trapping at the quench depth we considered in this paper: $k_BT/\varepsilon = 0.8$. However, if we quench more deeply—for example, $k_BT/\varepsilon = 0.1$— we do see trapping for both hydrodynamic and Brownian simulations. Chang and Yethiraj did not see trapping for their molecular dynamics simulations which explicitly include hydrodynamics. This discrepancy remains an interesting question. It may be because their chains are shorter (on real length scales) or because they include explicit solvent-polymer molecular interactions (which we do not).

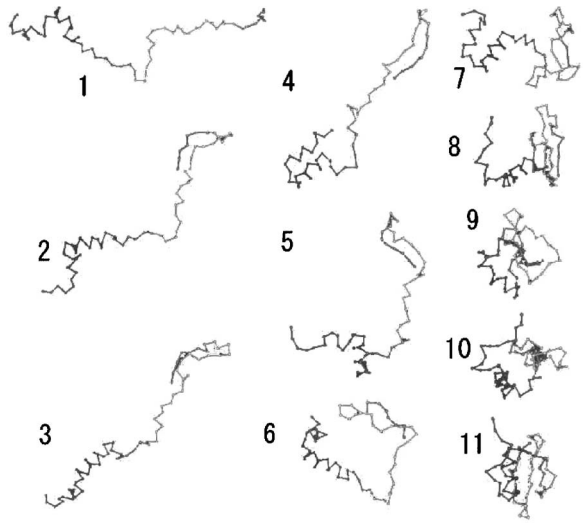

FIG. 9. A folding pathway for the protein 2*ci*2.

Abrams *et al.* [17] observed a similar collapse pathway for a $N=512$ chain quenched from a θ to a poor solvent using an explicit solvent and polymer molecular dynamics simulation. They analytically modeled early stage kinetics assuming a Gaussian fractal structure for the collapsing chain and successfully compared the analytical and numerical structure factor at early times. They also modeled later-stage kinetics assuming that the fractal structure persists and predicted hydrodynamic ($\tau_H \sim N^{5/6}$) and Brownian ($\tau_B \sim N^{3/2}$) collapse times at variance with those obtained here. The difference occurs because they assume a model of pearls connected by self-avoiding walks rather than linear chains. There is also interesting related work on the collapse of a polyelectrolyte [41] and of a constrained polymer [44].

Kuznetsov *et al.* [19,45] studied the collapse of a polymer quenched from a good to poor solvent using a Gaussian self-consistent method. Their numerical investigation showed three stages in the kinetics: namely, a rapid initial spinodal process, a long coarsening stage, and a final compaction-shape optimization stage. They found that the second stage dominates the collapse time for sufficiently long chains. The exponents given in Ref. [19] for collapse in a hydrodynamic (1.34 ± 0.03) and Brownian (1.96 ± 0.01) solvent agree with those presented here.

We may estimate the collapse time in a physical system using Eq. (15). The shear viscosity of water at 20 °C is $\eta \sim 1.0 \times 10^{-3}$ kg^{-1} s^{-1}. We take the size of a monomer to be $\sigma \sim 1.6 \times 10^{-9}$ m and the magnitude of the van der Waals interaction to be $\varepsilon \sim 2.0 \times 10^{-21}$ m^2 kg s^{-2}. Using these values we predict the collapse time for a typical polymer ($N \sim 10^4$) is $\tau_H \sim 10^{-4}$ s.

To summarize, we have shown that it is possible to follow the kinetics of the collapse transition of a polymer in a solvent using a hybrid mesoscale–molecular-dynamics algorithm. Hence it has been possible to show directly that hy-

drodynamic interactions speed up the collapse of the polymer chain as they enhance cooperative motion of the monomers. We have also presented a scaling argument describing the physical process responsible for the collapse kinetics. The predicted collapse times in a hydrodynamic ($\tau_H \sim N^{4/3}$) and Brownian heat bath ($\tau_B \sim N^2$) agree well with the numerical results ($\tau_H \sim N^{1.40\pm0.08}$ and $\tau_B \sim N^{1.89\pm0.09}$). The scaling theory predicts that the collapse time is proportional to the viscosity of the solvent and it would be of interest to check this experimentally.

In Sec. VI we examined the effect of hydrodynamics on the folding kinetics of proteins. We showed that for these systems, where many free energy minima compete, hydrodynamics has little effect on the kinetics as no cooperative flow is set up.

ACKNOWLEDGMENT

We would like to thank C. Micheletti for introducing us to the Go model.

[1] M. Doi and S. F. Edwards, *The Theory of Polymer Dynamics* (Clarendon Press, Oxford, 1986).
[2] P. G. de Gennes, *Scaling Concepts in Polymer Physics* (Cornell University Press, Ithica, NY, 1979).
[3] N. Kikuchi, A. Gent, and J. M. Yeomans, Eur. Phys. J. E **9**, 63 (2002).
[4] Z. Wang, J. Yu, and B. Chu, Macromolecules **25**, 1618 (1992).
[5] Q. Ying, B. Chu, and A. Yu. Grosberg, Macromolecules **28**, 180 (1995).
[6] P. W. Zhu and D. H. Napper, J. Chem. Phys. **106**, 6492 (1997).
[7] B. M. Baysal, N. Kayaman, E. E. Gurel, and F. E. Karaz, Macromolecules **32**, 8399 (1999).
[8] M. Nakata and T. Nakagawa, J. Chem. Phys. **110**, 2703 (1999).
[9] P. G. de Gennes, J. Phys. (France) Lett. **46**, L-639 (1985).
[10] B. Ostrovsky and Y. Bar-Yam, Europhys. Lett. **25**, 409 (1994).
[11] K. A. Dawson, E. G. Timoshenko, and P. Kiernan, Nuovo Cimento D **16**, 675 (1994).
[12] A. Buguin, F. Brochard Wyart, and P. G. de Gennes, C. R. Acad. Sci., Ser. IIb: Mec., Phys., Chim., Astron. **322**, 741 (1996).
[13] S. K. Nechaev, A. Yu. Grosberg, and E. I. Shakhnovich, J. Phys. (Paris) **49**, 2095 (1988).
[14] A. Halperin and P. M. Goldbart, Phys. Rev. E **61**, 565 (2000).
[15] A. Byrne, P. Kiernan, D. Green, and K. Dawson, J. Chem. Phys. **102**, 573 (1995).
[16] L. Klushin, J. Chem. Phys. **108**, 7917 (1998).
[17] C. F. Abrams, N. Lee, and S. Obukhov, Europhys. Lett. **59**, 391 (2002).
[18] E. Pitard, Eur. Phys. J. B **7**, 665 (1999).
[19] Y. A. Kuznetsov, E. G. Timoshenko, and K. A. Dawson, J. Chem. Phys. **104**, 3338 (1996).
[20] E. G. Timoshenko and K. A. Dawson, Phys. Rev. E **51**, 492 (1995).
[21] Y. A. Kuznetsov, E. G. Timoshenko, and K. A. Dawson, J. Chem. Phys. **102**, 1816 (1995).
[22] E. Pitard and H. Orland, Europhys. Lett. **41**, 467 (1998).
[23] Y. A. Kuznetsov, E. G. Timoshenko, and K. A. Dawson, J. Chem. Phys. **103**, 4807 (1995).
[24] B. Schnurr, F. C. Mackintosh, and D. R. M. Williams, Europhys. Lett. **51**, 279 (2000).
[25] R. Chang and A. Yethiraj, J. Chem. Phys. **114**, 7688 (2001).
[26] A. Malevanets and J. M. Yeomans, Europhys. Lett. **52**, 231 (2000).
[27] A. Malevanets and R. Kapral, J. Chem. Phys. **110**, 8605 (1999).
[28] M. Cieplak and T. X. Hoang, J. Biol. Phys. **26**, 273 (2000).
[29] H. Abe and N. Go, Biopolymers **20**, 1013 (1981).
[30] T. X. Hoang and M. Cieplak, J. Chem. Phys. **113**, 8319 (2000).
[31] M. S. Li and M. Cieplak, Phys. Rev. E **59**, 970 (1999).
[32] D. K. Klimov and D. Thirumalai, Proc. Natl. Acad. Sci. U.S.A. **97**, 2544 (2000).
[33] P. E. Rouse, J. Chem. Phys. **21**, 1272 (1953).
[34] B. H. Zimm, J. Chem. Phys. **24**, 269 (1956).
[35] K. Kremer and G. S. Grest, J. Chem. Phys. **92**, 5057 (1990).
[36] M. P. Allen and D. J. Tildesley, *Computer Simulation of Liquids* (Clarendon Press, Oxford, 1989).
[37] N. Kikuchi, C. M. Pooley, J. F. Ryder, and J. M. Yeomans, J. Chem. Phys. **119**, 6388 (2003).
[38] T. Ihle and D. M. Kroll, Phys. Rev. E **63**, 020201(R) (2001).
[39] M. Ripoll, K. Mussawisade, R. G. Winkler, and G. Gompper, Europhys. Lett. **68**, 106 (2004).
[40] N. Kikuchi, Ph.D. thesis, University of Oxford, 2003.
[41] N. Lee and S. Obukhov, Europhys. Lett. **66**, 350 (2004).
[42] A. Yu. Grosberg and A. R. Khokhlov, *Statistical Physics of Macromolecules* (Springer-Verlag, New York, 1984).
[43] F. C. Bernstein, T. F. Koetzle, G. J. B. Williams, E. F. Meyer, Jr., M. D. Brice, J. R. Rodgers, O. Kennard, T. Shimanouchi, and M. Tasumi, J. Mol. Biol. **112**, 535 (1977).
[44] I. S. Aranson and L. S. Tsimring, Europhys. Lett. **62**, 848 (2003).
[45] Y. A. Kuznetsov, E. G. Timoshenko, and K. A. Dawson, Physica A **257**, 61 (1998).